

Manipulation of charged domain walls in geometric improper ferroelectric thin films: A phase-field study

Amadé Bortis ^{*}, Morgan Trassin , Manfred Fiebig , and Thomas Lottermoser [†]
Department of Materials, ETH Zurich, 8093 Zurich, Switzerland



(Received 7 February 2022; accepted 18 May 2022; published 7 June 2022)

Using phase-field simulations, we show how interfaces acting on the geometric-improper ferroelectric polarization of hexagonal manganite and ferrite thin films can be used to control the formation of charged domain walls. We modify the Landau expansion of the free energy valid in bulk to emulate interface effects known from previous cross-sectional experiments, and we verify our model by comparing our results with images obtained in these experiments. We then show how the interface affects the orientation of ferroelectric domain walls in the fully three-dimensional case. Furthermore, we demonstrate that interface effects combined with an external electric field enable us to specifically choose the dominant domain-wall type (head-to-head, tail-to-tail, or neutral). We also find that an electric field can stabilize a novel domain-wall type which only emerges in the improper ferroelectric order but not in the primary structural distortion. Since the domain walls have a conductivity that is different from the interior of the domains, the influence of the interfaces of a thin film on the type and distribution of the walls gives us the possibility to control the transport properties of a material by appropriate thin-film engineering.

DOI: [10.1103/PhysRevMaterials.6.064403](https://doi.org/10.1103/PhysRevMaterials.6.064403)

I. INTRODUCTION

In geometric improper ferroelectrics such as the isostructural hexagonal manganites $RMnO_3$ ($R = \text{Sc, Y, In, Dy-Lu}$) and ferrites $RFeO_3$ ($R = \text{Y, Yb, Lu}$), a continuous phase transition causes a structural trimerization, which leads to a spontaneous, so-called improper, electric polarization as a secondary effect [1,2]. The resulting six trimerization-polarization domain states lead to unusual vortex domain patterns, where the polarization alternates around a vortex core [3,4]. This topologically protected arrangement can lead to charged ferroelectric domain walls with head-to-head and tail-to-tail arrangements of the polarization. These charged walls have been shown to exhibit an enhanced or reduced electrical conductivity with respect to the bulk, which is interesting for technological applications [5–8].

The recent progress in epitaxial growth of hexagonal manganite and ferrite thin films confirms that improper ferroelectricity can be carried over to films of only a few unit cells thickness [9,10]. A strong modification of the improper ferroelectric state at the interfaces of the films may occur, however. For example, $YMnO_3$ films grown on yttria-stabilized zirconia (YSZ) show a mechanical clamping of the lattice to the substrate [11]. This clamping suppresses the trimerization, and therefore also the polarization, in the first few unit cells away from the substrate. As another example, $YMnO_3$ films grown on Al_2O_3 form a buffer layer of YMn_2O_4 between the film and the substrate. The $YMnO_3/YMn_2O_4$ interface consists of a MnO double layer with a charge-ordered arrangement of Mn^{3+} and Mn^{2+} ions, which results in a preferred

direction of the polarization and its inducing trimerization at the interface [12]. In $LuFeO_3/LuFe_2O_4$ heterostructures the same effect was observed at every $LuFeO_3/LuFe_2O_4$ interface [13].

The use of such interface effects constitutes a promising route to promote the formation of the technologically relevant charged domain walls within the film. At this point, it is not known, however, how the interface effects might interfere with the likewise technologically relevant electric-field poling behavior. All that can be said for now is that the ferroelectric switching of the manganite thin films is basically possible [14–16]. For technological applications, a better understanding of how the particular conditions in thin films affect the manipulation of the ferroelectric domains and domain walls is therefore of great importance.

In this work, we derive models for the aforementioned suppression of the trimerization and charge ordering at the interfaces (henceforth referred to as “trimerization suppression” and “polarizing effect”, respectively) from phenomenological considerations. We employ phase-field simulations to study the consequences of the trimerization suppression and polarizing effect on the ferroelectric order in the films. In comparison to the bulk, we find a drastic change in the ferroelectric domain configuration and the density of charged domain walls in films of 4–20 unit cells. We then investigate how this domain configuration can be altered by an electric field, and we show that the interfaces affect the domain-wall-motion-driven electric poling to promote charged walls as the dominant type of domain walls in the film. In the case of the trimerization suppression, these charged walls occur in the polarization, but not in the trimerization phase, which is a type of domain wall that has so far not been observed in the $RMnO_3$ and $RFeO_3$ systems. In addition, we find that the interfaces cause a reduction of the coercivity and remanence of the films.

^{*}amade.bortis@mat.ethz.ch

[†]thomas.lottermoser@mat.ethz.ch

II. PHASE-FIELD MODELING

We use numerical methods since they provide a very general tool for the simulation of domain formation far beyond what is possible with analytical techniques. Phase-field simulations are an established tool in the investigation of ferroelectric materials in the continuum limit [17]. For the hexagonal manganites, a Landau expansion of the free energy describing the aforementioned trimerized phase has already been derived [18]. Since the hexagonal orthoferrites are isostructural and show the same type of trimerizing phase transition [2], their Landau expansion can be assumed to have the same form. Specifically, phase-field simulations employing this expansion have been used to study the bulk vortex domain structure in applied electric fields [19,20] or under strain [21,22] as well as the coupling of the trimerized-polar domains to the antiferromagnetic domains emerging at cryogenic temperatures [23]. To the best of our knowledge, however, this Landau expansion has so far not been adapted to describe thin films, something we will strive for in the following.

A. The bulk model

For comprehensiveness and in order to identify which of the coupling parameters are affected by interface effects, we begin by reviewing the Landau expansion that is valid for the bulk. There, a structural phase transition lowers the space-group symmetry from $P6_3/mmc$ to $P6_3cm$. In the manganites and ferrites, this transition involves a tilt of the MnO_5/FeO_5 bipyramids and leads to a trimerization of the crystal lattice. This trimerization is described by a complex order parameter field $\mathbf{Q} = \mathbf{Q}(\mathbf{r})$ with an amplitude $Q = Q(\mathbf{r})$ describing the magnitude of the tilt and a phase $\Phi = \Phi(\mathbf{r})$ describing the azimuthal tilt direction. Following the derivation by Artyukin *et al.* [18], the free energy density up to the sixth order in Q takes the form

$$f_{\mathbf{Q}}(\mathbf{r}) = \frac{a}{2}Q^2 + \frac{b}{4}Q^4 + \frac{Q^6}{6}(c + c' \cos 6\Phi). \quad (1)$$

The sixth-order term restricts the trimerization phase to six possible values $\Phi = 2\pi n/6$ with $n \in [0, 5]$, which minimize the free energy and lead to the emergence of six domain states. In terms of group theory, the trimerization is described by the zone-boundary mode K_3 [24] and corresponds to the tilting of the MnO_5 bipyramids as well as an opposite displacement of the rare-earth ions on their two different sites (2a and 4b in the Wyckoff notation). The trimerization is accompanied by the polar mode Γ_2^- [24] with amplitude $\mathcal{P} = \mathcal{P}(\mathbf{r})$, which induces an electric polarization $P_z \propto \mathcal{P}$ [18] along the z -axis. It interacts with the trimerization according to

$$f_{\mathcal{P}}(\mathbf{r}) = -gQ^3\mathcal{P} \cos 3\Phi + \frac{g'}{2}Q^2\mathcal{P}^2 + \frac{a_{\mathcal{P}}}{2}\mathcal{P}^2. \quad (2)$$

In line with the secondary nature of the polarization ($a_{\mathcal{P}} > 0$), the trimerization amplitude sets the magnitude of the polarization, and the phase sets its direction. Phases with even and odd values n are associated with up- and down-polarization states, respectively. The polarization interacts with an external electric field along the z -direction according to

$$f_E(\mathbf{r}) = -E\mathcal{P}. \quad (3)$$

Finally, a gradient term accounts for spatial variations in the order-parameter fields:

$$f_{\nabla}(\mathbf{r}) = \frac{1}{2} \sum_{i=x,y,z} [s_Q^i (\partial_i Q \partial_i Q + Q^2 \partial_i \Phi \partial_i \Phi) + s_{\mathcal{P}}^i \partial_i \mathcal{P} \partial_i \mathcal{P}]. \quad (4)$$

Here, ∂_i denotes the partial spatial derivative in the $i = x, y, z$ direction. Specifically, this gradient term sets the energetic cost for domain walls. The wall with the lowest energy is obtained for a shift in the trimerization phase of $\Delta\Phi = \pi/3$ across the wall [25]. Together with the sixth-order terms, this is the origin of the domain formation discussed before, where a vortex core is surrounded by alternatingly polarized domains corresponding to the six consecutive minima in the free energy with respect to n . We then obtain the free energy by integrating the total free energy density over the volume of the system,

$$F = \int d\mathbf{r} f(\mathbf{r}) = \int d\mathbf{r} [f_{\mathbf{Q}}(\mathbf{r}) + f_{\mathcal{P}}(\mathbf{r}) + f_E(\mathbf{r}) + f_{\nabla}(\mathbf{r})]. \quad (5)$$

In the following, we use $YMnO_3$ and its coupling parameters [18] as a representative for the hexagonal manganites and ferrites. To the best of our knowledge, these parameters have so far not been calculated for ferrites, but they can be safely assumed to be similar, because similar domain configurations have been observed [26]. Before we move on to include interface effects, we will briefly describe how the free energy in Eq. (5) is used to numerically simulate the formation of domain configurations in a film.

B. Computational details

To solve the phase-field model represented by Eq. (5) numerically, our film with a thickness L_z is described as a grid with dimensions $L_x \times L_y \times L_z$ and grid spacings of $h_x = h_y = 0.307$ nm and $h_z = 0.220$ nm, such that we can compare the dimensions of our simulated films to real ones ($2h_{x,y} = a, 5h_z = c$) [11]. For all films we simulate, we choose $L_x = L_y = 200$, and since the system is hexagonal, we thus simulate films that are about 130 unit cells wide. Initially, the order parameter fields $O_{1,2,3}(\mathbf{r}) = Q(\mathbf{r}), \Phi(\mathbf{r}), \mathcal{P}(\mathbf{r})$ are chosen to take random values on each grid point at $\mathbf{r} = (x, y, z)$. We then evolve the system according to the Ginzburg-Landau (GL) equations

$$\frac{\partial O_i}{\partial t}(\mathbf{r}, t) = -L \frac{\delta f(O_1(r), \dots, O_N(r))}{\delta O_i(\mathbf{r}, t)}. \quad (6)$$

Here, $\partial/\partial t$ denotes the partial derivative with respect to time, and $\delta f/\delta O_i$ denotes the derivative of the free-energy functional f with respect to the i th order parameter O_i . In the following, we set the mobility coefficient L to 1 as we focus on static properties. We use the calculation of the functional derivatives of Q , Φ , and \mathcal{P} as detailed in [19–21]. Evolving the system in time minimizes the free energy step by step and leads to the domain configurations observed in experiments. Since we are describing a z -oriented thin film, we use open boundary conditions along the z -axis and periodic boundary conditions along the x - and y -axes. Using finite differences, we discretize gradients with a seven-point stencil operator, which means that gradients at a grid point are calculated using only nearest-neighbor grid points. We perform the time

integration of the Ginzburg-Landau equations using the explicit Euler method and a time step of $\Delta t = 0.025$.

C. Interface effects in thin films

For both the trimerization suppression and the polarizing effect, we will now parametrize the effect introduced by the interface in a purely phenomenological way. The main purpose of this is to emulate the observed influence the interface has on the film, but not to identify and quantify the underlying microscopic sources. Our strategy is to make only minimal changes to the bulk Landau expansion. Indeed, we will show that by introducing a spatial dependence of just one coupling parameter, we can reproduce the experimentally obtained domain configurations for both the trimerization suppression and the polarizing effect in a satisfying way.

1. The trimerization suppression

The mechanical clamping of the film to the substrate was studied using density functional theory and experimentally using transmission electron microscopy [11]. Both approaches suggest that the amplitude Q of the trimerization is zero at the substrate interface and then increases steeply until it reaches the bulk value after only three unit cells. For our simulations, we emulate this behavior by a simple phenomenological relation satisfying $Q(z=0) = 0$ and $Q(z=3c) \approx Q_{\text{bulk}}$, where z is the distance from the substrate interface. This is achieved by introducing a spatial dependence on the parameter a in Eq. (1) according to

$$a(z) = a \tanh \frac{z - z_0}{z_Q}, \quad (7)$$

such that the sign of $a(z)$ switches at $z_0 = c$ and reaches the approximate bulk value of a after three unit cells by setting $z_Q = c$. We choose a hyperbolic tangent because it is a continuous function that offers two convenient parameters to tune the simulated trimerization suppression. This dependence, together with a depiction of how the minima in the free energy of Eq. (5) shift as z decreases, is shown in Fig. 1 for a film with $L_z = 4c$. Averaging the trimerization amplitude Q as a function of z recreates the onset of Q across three unit cells, as reported by Nordlander *et al.* [11].

2. The polarizing effect

Next, we emulate charge ordering as found at the top and bottom interfaces in $\text{LuFeO}_3/\text{LuFe}_2\text{O}_4$ heterostructures [12,13,26]. We thus consider a LuFeO_3 film with charge-ordered top and bottom interfaces. We know that this charge-ordering results in a preference for opposite polarization states at the top and bottom of the film, while the trimerization itself is not directly affected. Such an interface-induced polarization pinning can induce an electric field, as reported in the case of classical proper ferroelectric heterostructures [27]. Therefore, we emulate this preference with an effective electric field according to

$$f = -E(z)\mathcal{P}, \quad (8)$$

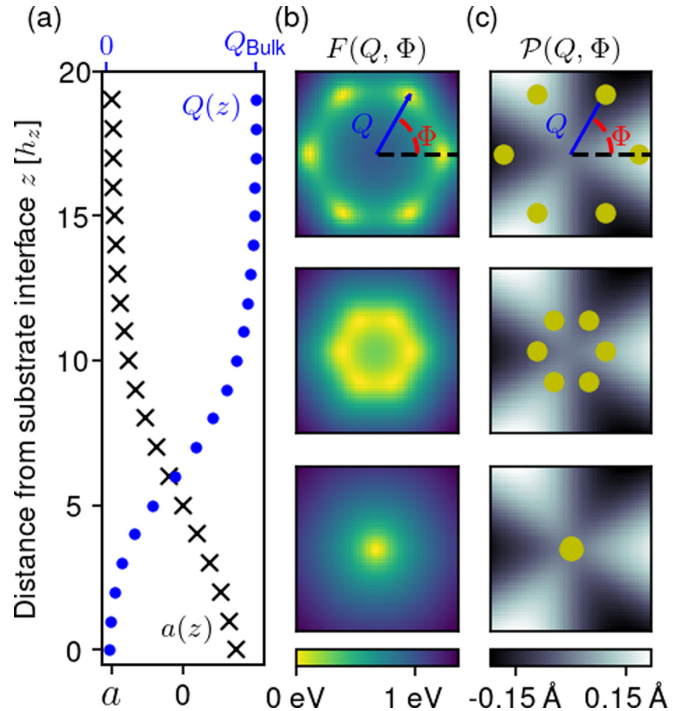


FIG. 1. (a) Coupling parameter a and trimerization amplitude Q in dependence on the distance z to the substrate interface. (b) Free energy in order parameter space for $z = 1h_z, 6h_z, 10h_z$ in (a). Note the shift of the minimum from $Q = 0$ to the six minima given by the bulk model when moving away from the substrate at $z = 0$. (c) Corresponding polarization in order parameter space. The locations of the minima in $F(Q, \Phi)$ (yellow points) identify the magnitude and sign of the polar displacement.

where the electric field is given by

$$E(z) = 0.5 \left(\tanh \frac{z - L_z - z_0}{z_E} + \tanh \frac{z - z_0}{z_E} \right). \quad (9)$$

Here, we assume that the charge order acts locally on the interface of the film so that we restrict this effective field to the first and last unit cell only. We achieve this by setting $z_0 = 5h_z$ and $z_E = 2h_z$, with the resulting dependence of E on z for a film with $L_z = 4c$ in Fig. 2. We can see that because we set opposite signs of $E(z)$ at the top ($z = L_z$) and bottom ($z = 0$) interfaces, the polarizations at these interfaces have opposite directions.

Note that all the changes we introduced to emulate the thin-film environment affect coefficients that are already present in the bulk model in Eq. (5), so that the equations of motion as such remain unchanged when moving from the bulk case toward thin films.

D. Model validation

Let us first verify if our modified Landau expansions recreate the experimentally observed features of the domain configuration in thin films. For the trimerization suppression, scanning transmission electron microscopy (STEM) measurements on a cross-section of the film revealed that the structural domain walls of the trimerization phase are oriented predominantly orthogonal to the substrate. No vortices were observed

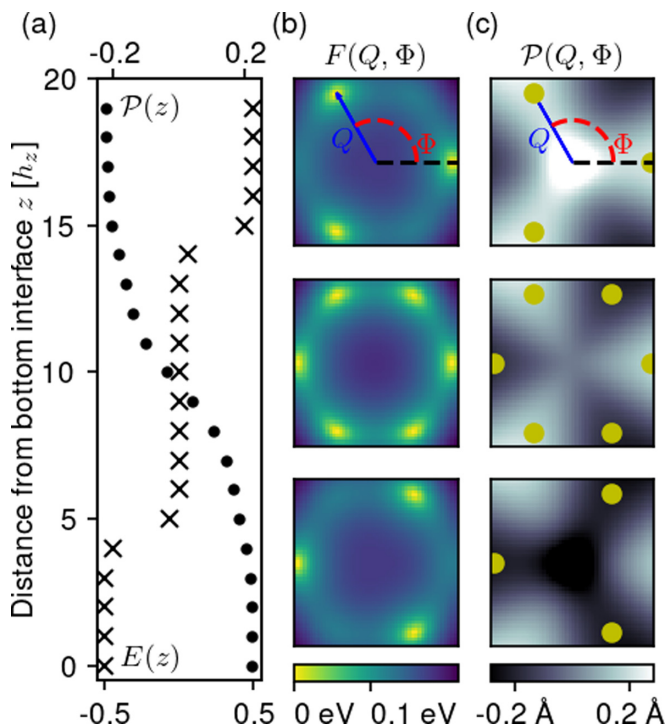


FIG. 2. (a) Effective electric field E and polarization \mathcal{P} in dependence on the distance z to the bottom interface. (b) Free energy in order parameter space for $z = 1h_z, 10h_z, 18h_z$ in (a). Note that at the top and bottom interfaces there is a threefold instead of a sixfold degeneracy due to the preference for one polarization direction. (c) Corresponding polarization in order-parameter space. The locations of the minima in $F(Q, \Phi)$ (yellow points) identify the magnitude and sign of the polar displacement.

in the measured cross-sections, but the topological protection in the arrangement of the domains is sustained in the form of stripe-domain configurations with a phase difference of $\Delta\Phi = \pi/3$ across any observed domain wall [11]. To compare our model to the experiment, we simulate a film with four unit cells thickness and iterate the Ginzburg-Landau equations for 2.5×10^4 steps. We extract the trimerization angle Φ and show a side view in Fig. 3(a). We clearly see that this is indeed consistent with the experimentally observed stripe domains. Apparently, the artificial spatial dependence imposed on $a(z)$ in Eq. (7) is sufficient to model the trimerization suppression.

For the polarizing effect, the structural domains observed by STEM exhibit a conical shape [13]. The preference of a specific interface polarization lifts the degeneracy associated with the six trimerization angles $\Phi = 2n\pi/6$, resulting in three degenerate domain states of equal polarization at lower energy and three more of opposite polarization at higher energy at the interface. The three domain states at higher energy are thus scarcely populated at the interface, but the resulting small domains expand laterally toward the opposite interface where these three states represent the ones at lower energy, thus explaining the conical shape of the domains. Following the same simulation procedure as before, we can extract a cross-section of the domain configuration; see Fig. 3(b). Again, our result agrees with the STEM images

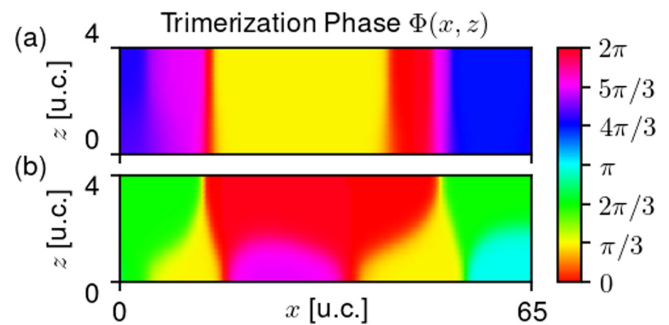


FIG. 3. Cross-section of a film of 4 u.c. in the xz -plane. We show the trimerization phase Φ for (a) the trimerization suppression and (b) the polarizing effect. For the trimerization suppression, we observe a stripe pattern of trimerization domains. Neighboring domains always show a difference in Φ of $\Delta\Phi = \pi/3$. The polarizing effect promotes domains with $\Phi = 0, 2\pi/3, 4\pi/3$ at the top and $\Phi = \pi/3, \pi, 5\pi/3$ at the bottom. As a result, conical domains are obtained.

and shows that the artificial spatial dependence imposed on $E(z)$ in Eq. (8) is sufficient to model the polarizing effect.

In summary, we see that our phenomenological emulations of the trimerization suppression and polarizing effect correctly reproduce the experimental result obtained with STEM. Hence, we now have an adequate tool to shed some light on the so far inaccessible fully three-dimensional domain configuration and on the polarization switching behavior in applied electric fields.

III. RESULTS

A. Ferroelectric domains

Now that we have verified that our model successfully replicates the domain configurations observed in the cross-sectional experiments, we expand our investigation to draw conclusions on the entire three-dimensional ferroelectric domain configuration and relate it to the conductance of the films. In particular, we explore how this domain configuration depends on the film thickness. We choose a lower limit to the thickness for all simulations, which asserts that the films reach their polar bulk structure, with the bulk value for the trimerization amplitude, for more than one unit cell. From experiments and simulations, we know that the bulk value of the trimerization amplitude is reached in the third unit cell [11]. On the other hand, bulklike behavior is obtained from about 20 unit cells. We therefore limit our investigations to the range from 4 to 40 unit cells.

1. Trimerization suppression

We start with the trimerization suppression for a film of four unit cells thickness, and we show the simulated ferroelectric domain configuration in Fig. 4(a). First of all, we notice that the vortex-domain pattern known from the bulk is preserved on the surface of the film. All ferroelectric domain walls are oriented parallel to the spontaneous polarization along the z -axis. From this we can already deduce that charged domain walls do not exist in a film of four unit cells. To investigate if a larger film thickness affects the orientation of

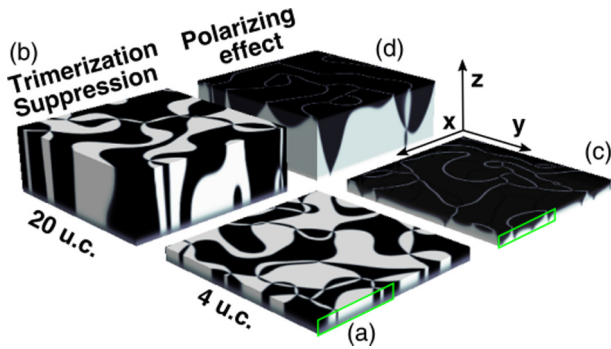


FIG. 4. Ferroelectric domain configuration in h -YMnO₃ thin films in a three-dimensional view. Films of 4 u.c. are shown for (a) the trimerization suppression and (c) the polarizing effect. Films of 20 u.c. are shown for (b) the trimerization suppression and (d) the polarizing effect. The green rectangles indicate the cross-section in Fig. 3.

the ferroelectric domain walls, we simulate a film with a thickness of 20 unit cells. As shown in Fig. 4(b), the ferroelectric domain walls now tend to bend away from the z -axis. This indicates that the increased thickness indeed promotes more charged walls.

To quantify the change of domain-wall type from neutral to charged, we define the density of charged walls ρ_{CDW} as the ratio of neighboring grid points separated by charged walls versus grid points separated by any type of domain wall. Because the polarization changes its direction only at a domain wall, we can calculate the number of pairs of grid points separated by a domain wall N_w by counting the number of sign changes of $\mathcal{P}(x, y, z)$ along the x -, y -, and z -axis. Note that by doing this, we assume that a charged wall can always be divided into horizontal and vertical segments, in agreement with experimental observations [28]. The polarization is oriented in the z -direction, therefore a sign change along z indicates a charged wall, while a sign change along x or y indicates a neutral wall. We can thus estimate the density of charged walls as

$$\rho_{\text{CDW}} = \frac{1}{N_w} \sum_{x,y=1}^{L_x, L_y} \sum_{z=1}^{L_z-1} |H(\mathcal{P}(x, y, z+1)) - H(\mathcal{P}(x, y, z))|, \quad (10)$$

where H is the Heaviside step function. We show ρ_{CDW} in dependence on the film thickness for the range between 4 and 40 unit cells in Fig. 5. From this graph, we conclude that the charged walls are suppressed ($\rho_{\text{CDW}} \approx 0$) for films with a thickness lower than 14 unit cells. Because charged walls in hexagonal manganites lead to an accumulation of mobile charge carriers at the wall (aside from band-bending effects), we can use ρ_{CDW} to estimate the conductance of the domain walls. Thus, the local domain-wall conductance of films below this threshold is solely governed by the neutral, vertical walls. Toward larger thickness, the films slowly recover the bulklike domain-wall network, consisting of a mixture of charged and neutral walls.

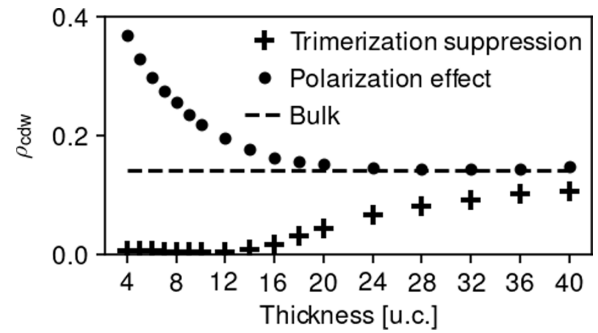


FIG. 5. The density of charged ferroelectric domain walls ρ_{CDW} as defined in Eq. (10) as a function of film thickness. The bulk value was obtained by simulating a film of 100 u.c. using periodic boundary conditions.

2. The polarizing effect

Next, we investigate the impact of the polarizing effect on the domain configuration, starting with a film of four unit cells as depicted in Fig. 4(c). The ferroelectric domains follow the conical structural domains induced by the preference for opposite polarization directions at the two interfaces described in Sec. II D. The conical domain shape implies an increased density of charged domain walls in comparison to the trimerization suppression. For the top surface in Fig. 4(c), we observe that despite the preference for a certain polarization direction, the opposite polarization domain state is still present at the surface so that the vortex domain pattern is preserved. We again turn our investigation toward thicker films. Figure 4(d) indicates that at increased thickness, films tend to exhibit an increased fraction of vertical, neutral walls. We now quantify this change in terms of ρ_{CDW} for a range of films with thicknesses between 4 and 40 unit cells, with the result shown in Fig. 5. The density of charged walls starts from a value of almost 40% and steadily decreases with increasing film thickness, reaching its bulk value at around 20 unit cells. Above this thickness, the interfaces do not promote a non-bulk-like density of charged walls, even though the domain structure itself is not yet bulklike; see Fig. 4.

3. Comparison of the trimerization suppression and the polarizing effect

We thus arrive at a complete picture of the thickness dependence of ρ_{CDW} for films with a trimerization suppression or polarizing effect. For the lowest considered thickness of four unit cells, the difference in ρ_{CDW} between films with a trimerization suppression or polarizing effect is the largest where the film with the trimerization suppression exhibits no charged walls at all and the film with the polarizing effect reaches a maximum of these. For both cases, ρ_{CDW} converges toward the bulk value with increasing film thickness, with the polarizing effect films reaching the bulk value faster than the films with the trimerization suppression. Since charged and neutral domain walls exhibit a different conductivity, thickness may therefore be used as a control parameter to engineer the overall conductance of the films.

B. Electric poling

Since it is vital for technological applications like logic devices to switch between states with a different conductance, we now expand our investigation to include ferroelectric switching in an external electric field. To investigate how our films react to such a field, we simulate hysteretic poling. The polarization interacts with this field according to Eq. (3). We choose a sinusoidal time dependence of the electric field according to

$$E(t) = E_0 \sin(ft), \quad (11)$$

with an amplitude $E_0 = 1.0$ and a frequency $f = 0.002$. Previous phase-field simulations [20] and experiments [29] for bulk systems identified domain-wall motion as the dominant mechanism promoting the ferroelectric poling. Because of the aforementioned topological protection, domains with a polarization (and corresponding trimerization) opposite to the applied field shrink down to narrow stripes. These stripes are persistent even far above the coercive field and act as natural expansion centers for ferroelectric domains of opposite polarization when the electric field is reversed. We will now explore how this switching mechanism works in the confined environment of a thin film.

1. Trimerization suppression

We first examine the ferroelectric switching in films of four unit cells thickness for the trimerization suppression. Starting from the film as shown in Fig. 4(a), we simulate one full hysteresis loop according to the procedure described in Sec. II A, with the results shown in Fig. 6(a). We are particularly interested in the impact of the suppressed trimerization at the interface on the switching process of the film. As discussed in Sec. II, the trimerization amplitude is reduced in the first three unit cells away from the substrate interface, and it takes on its approximate bulk value from the fourth layer. We calculate hysteresis curves for the top and bottom layers, which allows us to separate the impact of the trimerization suppression from the region dominated by bulklike behavior. We observe that the bottom layer has a lower coercivity and remanence than the top layer. This implies, as can be seen in Fig. 6(a), that the polarization reversal occurs first in the bottom layer (times t_1 – t_2), and later in the top layer (t_3 – t_4). Because the bottom and top layers have an opposite polarization direction between t_2 and t_3 , charged walls have to be present for a time $\Delta t \geq t_3 - t_2$. We confirm this by calculating the density of charged walls as a function of time using Eq. (10). In Fig. 6(b) we show the time dependence of ρ_{CDW} for one hysteresis cycle, and we see that $\rho_{\text{CDW}}(t)$ peaks at almost 50%. This means that temporarily, half of all the domain walls in the film are charged.

To track the evolution of the ferroelectric (\mathcal{P}) and trimerization (Φ) domains during the switching process, we show cross-sections of the film in addition to the hystereses. The cross-section of the remanent state at time t_1 reveals a stripe-domain configuration for Φ ; see Fig. 6(c). When the electric field is reversed toward $E < 0$ and further decreased from times t_2 to t_4 , we observe a broadening of the favorably polarized stripes via a lateral domain-wall motion. This lateral expansion of the stripe domains in Φ corresponds to the

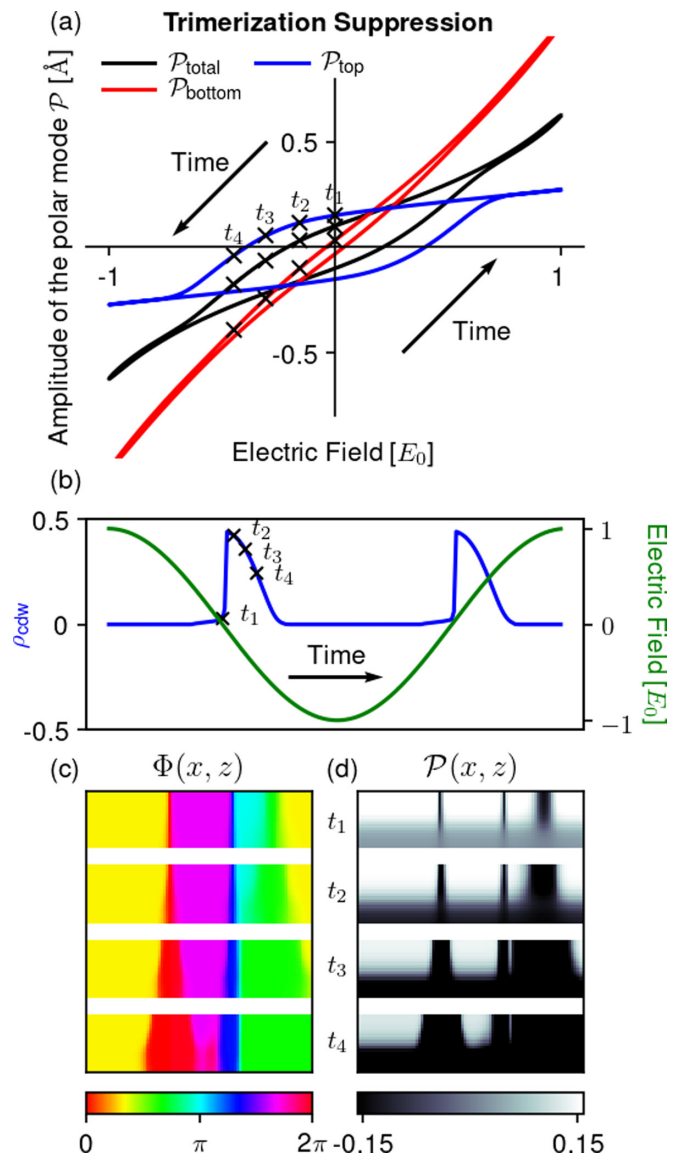


FIG. 6. (a) Ferroelectric hysteresis of a film of 4 u.c. with a trimerization suppression. The black curve shows the hysteresis curve for the whole film, and the red and blue curves show the hysteresis curve for a 1-u.c. layer at the bottom and top interfaces of the film, respectively. (b) Density of charged walls ρ_{CDW} as defined in Eq. (10) as a function of time for one hysteresis cycle. Cross-sections of the (c) trimerization and (d) polarization domains for four points in time as indicated in (a) and (b).

previously mentioned expansion of narrow stripes reported for bulk systems [20]. We observe this lateral wall motion for the \mathcal{P} domains as well; see Fig. 6(c). However, the hysteretic poling in Fig. 6(a) revealed a massive increase in the density of charged domain walls, which cannot be explained by lateral motion of neutral domain walls. And indeed, we observe an additional domain-wall motion upwards through the film from the substrate interface. As discussed, the bottom layer reverses its polarization before the rest of the film, and this creates charged walls in the films parallel to the substrate interface; see Fig. 6(c). It is important to note that this new wall only occurs in \mathcal{P} , but not Φ . This seems to indicate an unexpected

decoupling [11] of the secondary polarization mode Γ_2^- from the primary lattice-distortive mode K_3 . To facilitate our understanding, we use the Landau expansion in Eq. (5) and calculate the minimum free energy with respect to \mathcal{P} , yielding an expected polarization of

$$\mathcal{P} = \frac{gQ^3 \cos 3\Phi - E}{g'Q^2 + a_p}. \quad (12)$$

In this expression, we see that the polarization magnitude and direction depend on Q , E , and Φ . This implies that if Q is small enough, \mathcal{P} may reverse its sign for a sufficiently large magnitude of E while retaining its improper relation to the primary mode. The trimerization phase Φ does not change with \mathcal{P} because the cost in energy to create a new domain wall is proportional to Q^2 [see Eq. (4)]. For small values of Q , this is larger than the term proportional to Q^3 in Eq. (2) for the energy gain associated with changing Φ with \mathcal{P} , regardless of the values of the coupling strengths and domain-wall profile involved. In bulk, Q is large, and the corrections to the Γ_2^- displacement due to E are small, so that \mathcal{P} does not reverse its sign. In the thin film, Q is small close to the substrate interface. The E -field induced displacements can now reverse \mathcal{P} despite the 1:1 coupling of K_3 and Γ_2^- . This situation is sketched in Fig. 7(d) for the exemplary chosen displacements of the Y ion. In Figs. 7(a) and 7(b), we show the domain-wall profiles of Q , Φ , and \mathcal{P} for a bulk system and for the thin film extracted from the cross-sections in Fig. 6 at t_2 for $x = 0$. Note that in our case this wall is retained by energy minimization alone. In laboratory-grown samples, additional effects like pinning (fixing $Q = 0$ at the substrate interface) may stabilize this type of wall. The region in between the wall and the substrate also breaks the usual topological domain pattern in the polarization. It would be exciting to observe this predicted novel type of charged wall and the exact changes in ionic positions experimentally, but it has to be taken into account that this wall exists in an applied electric field only. With this new type of local ordering, the trimerization suppression may provide a reliable mechanism for creating charged walls, and thus effectively alter the conductance originating from domain walls of the film with an external electric field.

2. The polarizing effect

For the polarizing effect, we again simulate a hysteresis for the film of four unit cells thickness as shown in Fig. 4(c). As for the trimerization suppression, we calculate the hystereses for the top and bottom layers to see the impact of the interfaces. In Fig. 8(a), we show that the latter two hystereses are shifted towards negative electric fields and larger positive polarization for the top interface, and towards positive electric fields and larger negative polarization for the bottom interface. The shift in E is caused by the addition of a static electric field $E(z)$, which we use to emulate the preference in the polarization direction at the interfaces due to the charge ordering; see Eq. (9). Because $E(z)$ has a constant value of $+0.5$ at the top interface, the hysteresis curve gets shifted towards positive electric-field values. At the bottom interface, where $E(z) = -0.5$, the hysteresis curve gets shifted towards negative electric-field values. The shift towards larger positive (or negative) values of \mathcal{P} at the bottom (top) interface also has

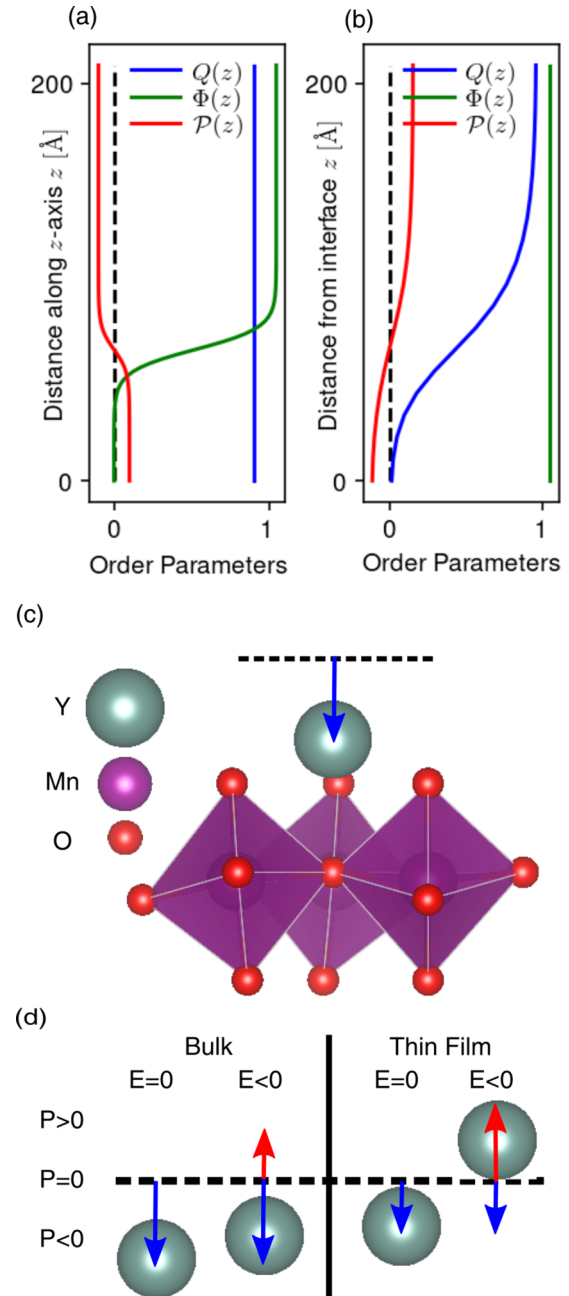


FIG. 7. (a) Order parameters Q , Φ , and \mathcal{P} in the z -direction for a domain wall in a bulk system. (b) Order parameters Q , Φ , and \mathcal{P} as a function of distance to the substrate interface for a thin film with a trimerization suppression. We extracted the order parameters from the cross-section at t_2 in Fig. 6. (c) Tilt of the MnO₅ bipyramids and the associated displacement of the Y ion in zero electric field for a bulk system. The dashed line indicates the Y position, which corresponds to $\mathcal{P} = 0$; the blue arrow indicates the total displacement of the Y ion. (d) Displacement of the same Y site for the bulk and thin-film case in zero and a finite electric field. The red arrow indicates the displacement caused by the electric field.

its origin in the value of $E(z)$, which leads to an imbalance in the preferred direction and magnitude of \mathcal{P} in fields of $+E$ versus $-E$.

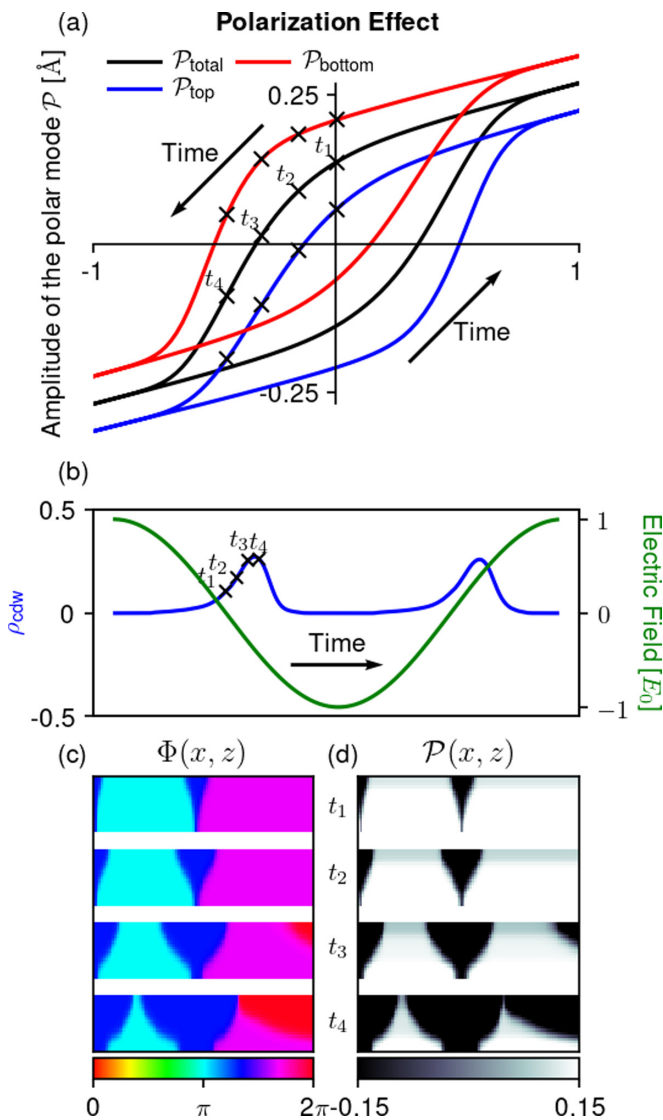


FIG. 8. (a) Ferroelectric hysteresis of a film of 4 u.c. with the polarizing effect. The black curve shows the hysteresis curve for the whole film, and the red and blue curves show the hysteresis curve for a 1-u.c. layer at the bottom and top interfaces of the film, respectively. (b) Density of charged walls ρ_{CDW} defined in Eq. (10) as a function of time for one hysteresis cycle. Cross-sections of the (c) trimerization and (d) polarization domains for four points in time as indicated in (a) and (b).

Note that the remanent polarization has the same sign at the top and bottom interfaces, implying a small density of charged walls. The polarization in the top layer is reversed at time t_2 , prior to the polarization reversal in the bottom layer, so that the density of charged domain walls in the film now has to increase. Macroscopically, this effect is similar to the one for the trimerization suppression. Indeed, when we calculate ρ_{CDW} as a function of time, we see an increase in ρ_{CDW} in the film during the time where \mathcal{P}_{top} and $\mathcal{P}_{\text{bottom}}$ point in opposite directions; see Fig. 8(b). When looking at the cross-section in Fig. 8(c), however, we see that the polarization and trimerization domains retain identical configurations. There is no independent sign reversal of \mathcal{P} as for the trimerization

suppression, because the trimerization amplitude Q keeps its bulk value for the polarizing effect. Thus, all walls in \mathcal{P} are also domain walls in Φ , just as is known from the bulk.

3. Comparison of the trimerization suppression and the polarizing effect

Let us briefly compare films with a trimerization suppression or polarizing effect in terms of the density of the charged walls they exhibit and how this density relates to the domain-wall conductance. The peak value of ρ_{CDW} reached during the hysteretic poling cycle is higher for the film with the trimerization suppression, where up to about 50% of all walls are charged, while for films with the polarizing effect this values never exceeds 30%. Because ρ_{CDW} gives the percentage of walls that are charged, we can use it to estimate the conductance of the domain walls. This is only an approximation, however, because the domain-wall conductance is a nonlinear function of the tilt angle and the domain-wall density that we do not scrutinize further. In addition, we cannot use ρ_{CDW} as a direct measure for the conductance of films. A comparison of the peak value of ρ_{CDW} will nevertheless be insightful in a discussion of possible device application.

4. Thickness-dependent hysteresis hallmarks

Thus far, we have discussed in detail how in YMnO_3 thin films the trimerization suppression and polarizing effect alter the polarization switching mechanism known from bulk specimens. These effects are, however, restricted to the first few unit cells away from an interface. In particular, the new type of charged wall found with the introduction of the trimerization suppression is only present close to the substrate interface, so that the resulting increase in ρ_{CDW} should become negligible for sufficiently thick films. We will investigate these issues by simulating hysteresis curves for films in a range between 4 and 40 unit cells thickness. We then extract the remanence, coercivity, and peak value of ρ_{CDW} , averaged over 100 independent runs, with the results shown in Fig. 9. We see that both remanence and coercivity steadily increase up to a thickness of about 20 unit cells for both the trimerization suppression and the polarizing effect, where they reach the bulk values. The peak density of charged walls drops with increasing thickness and reaches the bulk value around the same thickness. We can thus separate a thin-film regime, where the interface has a noticeable effect on the remanence, coercivity, and peak value of ρ_{CDW} , from a bulklike regime, where the interface effects become negligible, with a division between the two at a thickness of ≈ 20 unit cells.

IV. CONCLUSION

We used phase-field simulations to describe the domain configuration in geometric improper ferroelectric thin films, taking hexagonal manganites as a prominent example. We investigated two scenarios with different interface effects: suppression of the trimerization amplitude at the substrate interface, and charge ordering at the top and bottom interfaces. For both cases, we showed that while the bulklike vortex domain configuration is carried over to the thin films, the end points of the vortex strings appear predominantly on

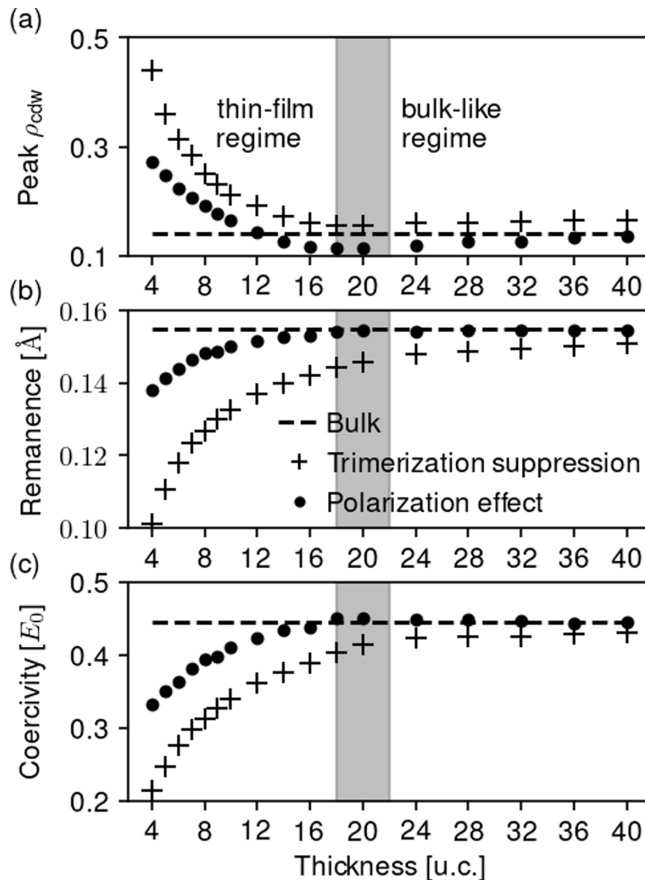


FIG. 9. (a) The peak value of the density of charged walls, (b) the remanent polarization, and (c) the coercive electric field as a function of film thickness. The bulk value was obtained from a simulation with a system of 100 u.c. thickness and periodic boundary conditions. The grey area indicates a transition from a thin-film regime into a bulklike regime at around 20 u.c., where all three quantities take approximately their bulk value.

the top surface of the film. This could explain the difficulty of experimentally finding vortices in vertical cross-sections of

the films. An electric field allows us to tune the density of charged walls by either promoting more bulklike charged walls that separate polarization and trimerization domains in the case of the polarizing effect, or by promoting a new type of charged domain wall that separates polarization but not trimerization domains in the case of the trimerization suppression. This does not express a decoupling of the trimerization and polarization modes K_3 and Γ_2^- , respectively, but rather an electric-field-induced reversal of the polarization amplitude while the K_3 - Γ_2^- coupling is maintained. This new type of wall is oriented parallel to the substrate and is likely to exhibit a different conductance from the bulklike walls. Films with the trimerization suppression exhibit a lower coercive field than films with the polarization effect, and thus they offer a greater potential for a sharp change in conductivity in smaller fields. While we mainly restricted ourselves to the discussion of static configurations, it might be interesting to include dynamical processes as they are introduced by phonons or frequency-dependent susceptibilities in the next step. But already from the simulated static configurations we can conclude that interface effects combined with an external electric field can be exploited to tune the conductance of the thin films via the type and density of charged walls. They play a crucial role in tuning technologically relevant parameters of geometrically improper ferroelectric thin films, such as their transport properties or the energy required for polarization switching.

ACKNOWLEDGMENTS

We thank Johanna Nordlander for fruitful discussions and comments on the manuscript. All simulations were performed on the Euler cluster at ETH Zurich. This research was supported by the EU European Research Council under Advanced Grant Program, No. 694955-INSEETO. We also acknowledge financial support by the Swiss National Science Foundation under Project No. 200021-178825. MT acknowledges financial support by the Swiss National Science Foundation under Project No 200021-188414.

- [1] B. B. Van Aken, T. T. M. Palstra, A. Filippetti, and N. A. Spaldin, *Nat. Mater.* **3**, 164 (2004).
- [2] E. Magome, C. Moriyoshi, Y. Kuroiwa, A. Masuno, and H. Inoue, *Jpn. J. Appl. Phys.* **49**, 09ME06 (2010).
- [3] T. Choi, Y. Horibe, H. T. Yi, Y. J. Choi, W. Wu, and S.-W. Cheong, *Nat. Mater.* **9**, 253 (2010).
- [4] K. Du, B. Gao, Y. Z. Wang, X. H. Xu, J. W. Kim, R. W. Hu, F. T. Huang, and S.-W. Cheong, *npj Quantum Mater.* **3**, 33 (2018).
- [5] D. Meier, J. Seidel, A. Cano, K. Delaney, Y. Kumagai, M. Mostovoy, N. A. Spaldin, R. Ramesh, and M. Fiebig, *Nat. Mater.* **11**, 284 (2012).
- [6] E. Ruff, S. Krohns, M. Lilienblum, D. Meier, M. Fiebig, P. Lunkenheimer, and A. Loidl, *Phys. Rev. Lett.* **118**, 036803 (2017).
- [7] D. R. Småbråten, Q. N. Meier, S. H. Skjærvø, K. Inzani, D. Meier, and S. M. Selbach, *Phys. Rev. Mater.* **2**, 114405 (2018).
- [8] D. Meier and S. M. Selbach, *Nat. Rev. Mater.* **7**, 157 (2022).
- [9] Z. Sheng, N. Ogawa, Y. Ogimoto, and K. Miyano, *Phys. Rev. B* **84**, 140101(R) (2011).
- [10] W. Wang, J. Zhao, W. Wang, Z. Gai, N. Balke, M. Chi, H. N. Lee, W. Tian, L. Zhu, X. Cheng, D. J. Keavney, J. Yi, T. Z. Ward, P. C. Snijders, H. M. Christen, W. Wu, J. Shen, and X. Xu, *Phys. Rev. Lett.* **110**, 237601 (2013).
- [11] J. Nordlander, M. Campanini, M. D. Rossell, R. Erni, Q. N. Meier, A. Cano, N. A. Spaldin, M. Fiebig, and M. Trassin, *Nat. Commun.* **10**, 5591 (2019).
- [12] S. Cheng, C. Xu, S. Deng, M.-G. Han, S. Bao, J. Ma, C. Nan, W. Duan, L. Bellaiche, Y. Zhu, and J. Zhu, *Sci. Adv.* **4**, eaar4298 (2018).
- [13] M. E. Holtz, E. S. Padgett, R. Steinhardt, C. M. Brooks, D. Meier, D. G. Schlom, D. A. Muller, and J. A. Mundy, *Phys. Rev. Lett.* **126**, 157601 (2021).
- [14] D. Lee, A. Yoon, S. Y. Jang, J.-G. Yoon, J.-S. Chung, M. Kim, J. F. Scott, and T. W. Noh, *Phys. Rev. Lett.* **107**, 057602 (2011).

- [15] T. Yoshimura, N. Fujimura, and T. Ito, *Appl. Phys. Lett.* **73**, 414 (1998).
- [16] D. Ito, N. Fujimura, and T. Ito, *Jap. J. Appl. Phys.* **39**, 5525 (2000).
- [17] J.-J. Wang, B. Wang, and L.-Q. Chen, *Ann. Rev. Mater. Res.* **49**, 127 (2019).
- [18] S. Artyukhin, K. T. Delaney, N. A. Spaldin, and M. Mostovoy, *Nat. Mater.* **13**, 42 (2013).
- [19] F. Xue, X. Wang, I. Socolenco, Y. Gu, L.-Q. Chen, and S.-W. Cheong, *Sci. Rep.* **5**, 17057 (2015).
- [20] K. L. Yang, Y. Zhang, S. H. Zheng, L. Lin, Z. B. Yan, J.-M. Liu, and S.-W. Cheong, *Phys. Rev. B* **96**, 144103 (2017).
- [21] F. Xue, X. Wang, Y. Shi, S.-W. Cheong, and L.-Q. Chen, *Phys. Rev. B* **96**, 104109 (2017).
- [22] X. Shi, H. Huang, and X. Wang, *J. Alloys Compd.* **719**, 455 (2017).
- [23] M. Giraldo, Q. N. Meier, A. Bortis, D. Nowak, N. A. Spaldin, M. Fiebig, M. C. Weber, and T. Lottermoser, *Nat. Commun.* **12**, 3093 (2021).
- [24] C. J. Fennie and K. M. Rabe, *Phys. Rev. B* **72**, 100103(R) (2005).
- [25] Y. Kumagai and N. A. Spaldin, *Nat. Commun.* **4**, 1540 (2013).
- [26] J. A. Mundy, C. M. Brooks, M. E. Holtz, J. A. Moyer, H. Das, A. F. Rébola, J. T. Heron, J. D. Clarkson, S. M. Disseler, Z. Liu *et al.*, *Nature (London)* **537**, 523 (2016).
- [27] A. K. Tagantsev and G. Gerra, *J. Appl. Phys.* **100**, 051607 (2006).
- [28] Y. Yu, X. Zhang, Y. G. Zhao, N. Jiang, R. Yu, J. W. Wang, C. Fan, X. F. Sun, and J. Zhu, *Appl. Phys. Lett.* **103**, 032901 (2013).
- [29] A. Ruff, Z. Li, A. Loidl, J. Schaab, M. Fiebig, A. Cano, Z. Yan, E. Bourret, J. Glaum, D. Meier, and S. Krohns, *Appl. Phys. Lett.* **112**, 182908 (2018).